


 Cite this: *RSC Adv.*, 2020, **10**, 22856

Biguanide–transition metals complexes as potential drug for hyperglycemia treatment †‡

 Stephanny Villamizar-Delgado,^{ab} Laura M. Porras-Osorio,^a Octavio Piñeros,^a Javier Ellena,^c Norman Balcazar,^{de} Ruben E. Varela-Miranda^a and Richard F. D’Vries^{id}*^a

Coordination compounds of Cu(II), Ni(II), Co(II), and Zn(II) with a type of biguanide (known commercially as metformin) have been synthesized and characterized using spectroscopic techniques (FT-IR, UV/VIS), X-ray diffraction techniques and thermal analysis. For all compounds, single crystals were obtained for single-crystal X-ray diffraction. For the first time, an octahedral cobalt compound with the formula $[\text{Co}(\text{C}_4\text{H}_{11}\text{N}_5)_3]\text{Cl}_2 \cdot 2\text{H}_2\text{O}$ that crystallizes in the monoclinic space group $C2/c$ with one molecule in the asymmetric unit has been obtained. Also, a novel nickel compound with the formula $[\text{Ni}(\text{C}_4\text{H}_{11}\text{N}_5)(\text{C}_4\text{H}_{10}\text{N}_5)]\text{Cl} \cdot \text{H}_2\text{O}$ that crystallizes in the monoclinic space group $P2_1/c$ with two molecules in the asymmetric unit was obtained. Finally, we obtained copper and zinc compounds that crystallize in the monoclinic space groups $P2_1/n$ and $P2_1/c$ with the general formula $[\text{Cu}(\text{C}_4\text{H}_{11}\text{N}_5)_2]\text{Cl}_2 \cdot \text{H}_2\text{O}$ and $[\text{Zn}(\text{C}_4\text{H}_{12}\text{N}_5)\text{Cl}_3]$, respectively. A structural and supramolecular analysis was developed for all compounds using Hirshfeld surface analysis and electrostatic potential maps. The cell viability of the obtained compounds was evaluated in C2C12 (ATCC CRL-1772™) mouse muscle cells and HepG2 (ATCC HB-8065™) human liver carcinoma cells by the MTT assay to determine the potential of the compounds as new safe drugs. The results demonstrate that the compounds exhibit low cytotoxicity at doses less than $250 \mu\text{g mL}^{-1}$ with a cell viability greater than 80%.

 Received 5th May 2020
 Accepted 27th May 2020

DOI: 10.1039/d0ra04059b

rsc.li/rsc-advances

Introduction

About 100 million people worldwide have type II diabetes (T2D), making it one of the most common chronic diseases.¹ Diabetes is characterized by a high concentration of glucose in the blood (hyperglycemia) due to the excessive production of liver glucose and resistance to peripheral insulin.² Currently, the underlying causes of these physiological behaviors are not well understood, but diabetes is known to be associated with both genetic and acquired factors, such as unhealthy eating habits, stress, hypertension, obesity, sedentary lifestyle, and metabolic

syndrome.¹ Of these, hyperglycemia is considered the leading risk factor for the development of diabetic complications.

Currently, one of the most widely used pharmaceutical compounds to control hyperglycemia in patients with T2D is metformin hydrochloride (a biguanide derivative) due to its effectiveness and good safety profile.³ However, it is also associated with adverse side effects, including lactic acidosis, and can cause serious problems in patients with cardiovascular, renal, hepatic, and pulmonary disease.⁴

One pharmaceutical alternative for the treatment of diabetes, metabolic syndrome, cancer, bacterial, fungal and viral infections, and other diseases is the use of metallo-drugs.⁵ Metallo-drugs are pharmacological compounds that contain an organic molecule coordinated to a metallic center.⁶ In this sense, different metallo-drugs complexes form from metformin are obtained and tested its biological activity against different micro-organism.^{7,8} Also, are reported patents that involve the metformin and metals as chromium and vanadium in the treatment of T2D and metabolism disorders.⁹ In other hand, has been demonstrated the activity of different metallo-drugs based in V(V), Cr(III), Mo(VI), W(VI), Zn(II), Cu(II), and Mn(III) in the treatment of diabetes and metabolic syndromes.¹⁰ This type of compound can act in two different ways: (i) the metal–organic complex exhibits the biological activity over a biological target, and (ii) the complex act as a carrier to transport the organic

^aFacultad de Ciencias Básicas, Universidad Santiago de Cali, Calle 5 #62-00, Cali, Colombia. E-mail: richard.dvries00@usc.edu.co

^bSão Carlos Institute of Chemistry, University of São Paulo, CEP 13.566-590, São Carlos, SP, Brazil

^cSão Carlos Institute of Physics, University of São Paulo, CEP 13.566-590, São Carlos, SP, Brazil

^dMolecular Genetics Group, Universidad de Antioquia, Calle 70, No 52-21, A. A. 1226, Medellín, Colombia

^eDepartment of Physiology and Biochemistry, School of Medicine, Universidad de Antioquia, Calle 70, No 52-21, A. A. 1226, Medellín, Colombia

† The results reported in this work are under United States Patent and Trademark Office (USPTO) US62884597.

‡ Electronic supplementary information (ESI) available: IR spectra and TGA-DSC analysis for all compounds. CCDC 1998783–1998786. For ESI and crystallographic data in CIF or other electronic format see DOI: 10.1039/d0ra04059b



molecule to the active site and produce the therapeutic activity. In both cases, the synergic action of the components improves the biological activity while minimizing the side effects.

Our research group has focused on the development of new molecules and metallo-drugs as pharmaceutical alternatives for the treatment of multiples diseases, such as T2D and metabolic syndrome.^{11–13} Several attempts to obtain metformin–metal complexes have been reported, but in most cases, the structural data could not be obtained, and in others, an incomplete structural analysis was performed.^{7,14–16}

To address these shortcomings, this work focuses on the synthesis, characterization, and structural study of complexes based on metformin and transition metals, including Co(II), Cu(II), Ni(II), and Zn(II). We aim to make a first close-up of the cytotoxic activity in order to propose new therapeutic alternatives in the treatment of T2D and metabolic syndrome.

Experimental section

General information

The following reagents and solvents were commercially available and used as supplied without further purification: metformin hydrochloride U. S. P. (Metf) (Harman Finocem Limited); $\text{CoCl}_2 \cdot 6\text{H}_2\text{O}$ (99%, Sigma-Aldrich); $\text{CuCl}_2 \cdot 2\text{H}_2\text{O}$ (99%, Sigma-Aldrich); $\text{NiSO}_4 \cdot 6\text{H}_2\text{O}$ (99%, Sigma-Aldrich); and $\text{ZnCl}_2 \cdot 6\text{H}_2\text{O}$ (99%, Sigma-Aldrich). Chemical and reagents used in cell culture included phosphate-buffered saline $1 \times$ (PBS) (Gibco, Carlsbad, CA, USA), low glucose Dulbecco's Modified Eagle's Medium (LGDMEM) (Sigma-Aldrich, St. Louis, MO, USA), high glucose Dulbecco's Modified Eagle's Medium (HGDMEM) (Sigma-Aldrich, St. Louis, MO, USA), RPMI 1640 Medium (Sigma-Aldrich, St. Louis, MO, USA), fetal bovine serum (FBS) (Invitrogen, Carlsbad, CA, USA), penicillin–streptomycin (P/S) $10\,000\ \text{U mL}^{-1}$ (Invitrogen, Carlsbad, CA, USA), glutamine (Gibco, Carlsbad, CA, USA), and the methyl thiazole tetrazolium (MTT) assay (Amresco, Solon, OH, USA).

Thermogravimetric analysis (TGA) was performed in a TA instrument (Discovery SDT 650) under the following conditions: 25–900 °C temperature range, under nitrogen ($100\ \text{mL min}^{-1}$ flow) atmosphere, and $20\ \text{°C min}^{-1}$ heating rate. Fourier-transform infrared spectrophotometry (FTIR) spectra were recorded from KBr pellets in the $4000\text{--}250\ \text{cm}^{-1}$ range on a Shimadzu IRAffinity-1.

Synthesis of the $[\text{Co}(\text{C}_4\text{H}_{11}\text{N}_5)_3]\text{Cl}_2 \cdot 2\text{H}_2\text{O}$ complex (compound 1)

In a flat-bottomed flask, 10 mL of methanolic solutions of the Mfn ligand ($\text{C}_4\text{H}_{12}\text{N}_5\text{Cl}$) (33 mg, 0.2 mmol) were mixed with 1.2 equivalents of NaOH and 5 mL of cobalt(II) chloride ($\text{CoCl}_2 \cdot 6\text{H}_2\text{O}$) (23 mg, 0.1 mmol). The reaction mixture was refluxed for 60 minutes. The resulting solution was concentrated and cooled to room temperature. Cubic reddish crystals were obtained by slow evaporation after 4 weeks (yield = 61.57%). Elemental anal. calcd for $[\text{Co}(\text{C}_4\text{H}_{11}\text{N}_5)_3]\text{Cl}_2 \cdot 2\text{H}_2\text{O}$ ($\text{C}_{12}\text{H}_{37}\text{N}_{15}\text{O}_2\text{Cl}_2\text{Co}$): C, 26.05; H, 6.74; N, 37.97. Found: C, 25.86; H, 6.02; N, 37.21.

Synthesis of the $[\text{Ni}(\text{C}_4\text{H}_{11}\text{N}_5)(\text{C}_4\text{H}_{10}\text{N}_5)]\text{Cl} \cdot \text{H}_2\text{O}$ complex (compound 2)

In a flat-bottomed flask, 4 mL of a solution of the Mfn ligand ($\text{C}_4\text{H}_{12}\text{N}_5\text{Cl}$) (66 mg 0.4 mmol) were mixed with 4 mL of aqueous nickel(II) sulfate solution ($\text{NiSO}_4 \cdot 6\text{H}_2\text{O}$) (47 mg, 0.2 mmol) and 53 mg of NaOH (1.3 mmol). The reaction mixture was stirred for 60 minutes at room temperature. The resulting solution was cooled to room temperature and filtered to separate the orange solid (crystalline powder) obtained. The obtained solid was dissolved in water, and HCl was added dropwise until dissolution. The compound was recrystallized by slow evaporation to obtain prism orange crystals (yield = 53.70%). Elemental anal. calcd for $[\text{Ni}(\text{C}_4\text{H}_{11}\text{N}_5)(\text{C}_4\text{H}_{10}\text{N}_5)]\text{Cl} \cdot \text{H}_2\text{O}$ ($\text{C}_8\text{H}_{23}\text{N}_{10}\text{OClNi}$): C, 26.01; H, 6.27; N, 37.91. Found: C, 25.67; H, 5.81; N, 37.03.

Synthesis of the $[\text{Cu}(\text{C}_4\text{H}_{11}\text{N}_5)_2]\text{Cl}_2 \cdot 2\text{H}_2\text{O}$ complex (compound 3)

In a flat-bottomed flask, 4 mL of an aqueous solution of the Mfn ligand ($\text{C}_4\text{H}_{12}\text{N}_5\text{Cl}$) (33 mg, 0.2 mmol) were mixed with 4 mL of an aqueous solution of copper(II) chloride ($\text{CuCl}_2 \cdot 2\text{H}_2\text{O}$) (200 mg, 1.17 mmol) and 1.2 equivalents of NaOH. The reaction mixture was stirred for 60 minutes at room temperature. The resulting solution was concentrated, cooled to room temperature, and filtered to obtain a purple solid. The solid was dissolved in water and recrystallized by slow evaporation to obtain purple needless crystals (yield = 88.02%). Elemental anal. calcd for $[\text{Cu}(\text{C}_4\text{H}_{11}\text{N}_5)_2]\text{Cl}_2 \cdot 2\text{H}_2\text{O}$ ($\text{C}_8\text{H}_{26}\text{N}_{10}\text{OCl}_2\text{Cu}$): C, 22.41; H, 6.11; N, 32.66. Found: C, 22.15; H, 6.21; N, 32.41.

Synthesis of the $[\text{Zn}(\text{C}_4\text{H}_{12}\text{N}_5)\text{Cl}_3]$ complex (compound 4)

In a flat-bottomed flask, 4 mL of an aqueous solution of the Mfn ligand ($\text{C}_4\text{H}_{12}\text{N}_5\text{Cl}$) (119 mg, 0.72 mmol) were mixed with 4 mL of an aqueous solution of zinc(II) chloride (ZnCl_2) (200 mg, 1.46 mmol) and 1.2 equivalents of NaOH. The reaction mixture was stirred for 2.5 hours at room temperature. The resulting solution was filtered to obtain a colorless solid. The solid was dissolved in water and recrystallized by slow evaporation to obtain colorless crystals (yield = 60.15%). Elemental anal. calcd for $[\text{Zn}(\text{C}_4\text{H}_{12}\text{N}_5)\text{Cl}_3]$ ($\text{C}_4\text{H}_{12}\text{N}_5\text{Cl}_3\text{Zn}$): C, 15.91; H, 4.01; N, 23.20. Found: C, 15.56; H, 3.98; N, 23.11.

Single-crystal X-ray diffraction (SCXRD) for structure determination

SCXRD data for all compounds were collected at room temperature (293 K) on a Rigaku XTALAB-MINI diffractometer using $\text{MoK}\alpha$ radiation ($0.71073\ \text{Å}$) monochromated by graphite. The cell determination and final cell parameters were obtained on all reflections using CrysAlisPro software.¹⁷ Data integration and scaling were performed using CrysAlisPro software.¹⁷ The structures were solved and refined with SHELXT¹⁸ and SHELXL¹⁹ softwares, respectively, including in Olex2.²⁰ In all cases, non-hydrogen atoms were clearly resolved and full-matrix least-squares refinement with anisotropic thermal parameters was performed. In addition, hydrogen atoms were stereochemically positioned and refined using the riding model in all cases.²¹ The Co compound was refined using the Squeeze routine (Platon)²² to



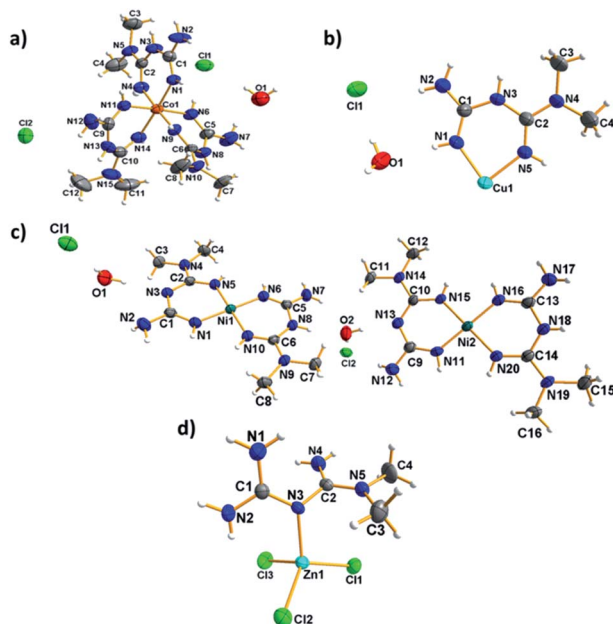


Fig. 1 ORTEP type diagram of the asymmetric unit for the compounds: (a) $[\text{Co}(\text{C}_4\text{H}_{11}\text{N}_5)_3]\text{Cl}_2 \cdot 2\text{H}_2\text{O}$, (b) $[\text{Cu}(\text{C}_4\text{H}_{11}\text{N}_5)_2]\text{Cl}_2 \cdot \text{H}_2\text{O}$, (c) $[\text{Ni}(\text{C}_4\text{H}_{11}\text{N}_5)(\text{C}_4\text{H}_{10}\text{N}_5)]\text{Cl} \cdot \text{H}_2\text{O}$ and (d) $[\text{Zn}(\text{C}_4\text{H}_{12}\text{N}_5)\text{Cl}_3]$ showing 50% of probability ellipsoids.

decrease the disorder solvent contribution (water in our case) to calculate the structure factors and improve the refinement values. Oak Ridge Thermal Ellipsoid Plot (ORTEP) diagrams for all structures were prepared with Diamond.²³ Mercury program were used for the preparation of artwork.²⁴

Cell cultures

C2C12 (ATCC CRL-1772TM) mouse muscle cells and HepG2 (ATCC HB-8065TM) human liver carcinoma cells were purchased from the American Type Culture Collection (ATCC) (Manassas, VA, USA). Cells were cultured at 37 °C and 5% CO_2 in DMEM supplemented with 10% FBS, 2 mM glutamine, penicillin, and 1% streptomycin (Sigma). When C2C12 cells reached 80–90% confluency, they were differentiated into myotubes using low glucose DMEM (5.5 mM) supplemented with 5% horse serum (HS).²⁵

To evaluate cell viability, HepG2 and C2C12 cells were seeded in 96 multi-well plates at a density of 2.5×10^4 cells per well and cultured for 24 h. The cells were washed once with DMEM and then incubated with different concentrations of extracts or fractions (1000, 500, 250, 125, 62.5, 31.25 $\mu\text{g mL}^{-1}$) in DMEM for 4 h (C2C12) or 48 h (HepG2). The negative control is formed by cell culture medium with the same cell concentration and 0.05% of DMSO. Insulin 0.3 mM (INS) and metformin 5 mM (MET) are used as positive control. Subsequently, the medium was removed, cells were washed once, and MTT (5 mg mL^{-1}) in DMEM was added to each well and incubated for 4 h. The MTT-containing medium was removed, and 200 μL of DMSO were added to dissolve the formazan crystals. The optical densities (OD) were measured using a Varioskan Flash spectrophotometer (Thermo, Waltham, MA, USA) at 570 nm.²⁶

Results and discussion

ORTEP type diagrams of the asymmetric unit for all compounds are shown in Fig. 1. The hydrogen atoms for all compounds are

Table 1 Crystallographic data and refinement parameters for (1) $[\text{Co}(\text{C}_4\text{H}_{11}\text{N}_5)_3]\text{Cl}_2 \cdot 2\text{H}_2\text{O}$, (2) $[\text{Ni}(\text{C}_4\text{H}_{11}\text{N}_5)(\text{C}_4\text{H}_{10}\text{N}_5)]\text{Cl} \cdot \text{H}_2\text{O}$, (3) $[\text{Cu}(\text{C}_4\text{H}_{11}\text{N}_5)_2]\text{Cl}_2 \cdot \text{H}_2\text{O}$ and (4) $[\text{Zn}(\text{C}_4\text{H}_{12}\text{N}_5)\text{Cl}_3]$ compounds

Compound	(1)	(2)	(3)	(4)
Emp. formula	$\text{C}_{12}\text{H}_{33}\text{N}_{15}\text{Co}, 2(\text{Cl}), \text{H}_2\text{O}$	$\text{C}_{16}\text{H}_{42}\text{N}_{20}\text{Ni}_2, 2(\text{Cl}), 2\text{H}_2\text{O}$	$\text{C}_8\text{H}_{22}\text{N}_{10}\text{Cu}, 2(\text{Cl}), 2(\text{H}_2\text{O})$	$\text{C}_4\text{H}_{12}\text{Cl}_3\text{N}_5\text{Zn}$
FW (g mol^{-1})	535.38	739.05	428.83	301.91
Crystal system	Monoclinic	Monoclinic	Monoclinic	Monoclinic
Space group	$C2/c$	$P2_1/c$	$P2_1/n$	$P2_1/c$
Unit cell				
a (Å)	36.470(2)	13.3863(6)	5.1596(14)	12.5200(12)
b (Å)	8.5892(6)	7.4187(5)	11.562(2)	7.5140(6)
c (Å)	17.3656(13)	15.7512(9)	15.091(4)	13.0298(13)
β (°)	99.376(6)	104.757(5)	95.63(3)	113.199(12)
Volume (Å ³)	5367.1(6)	1512.64(15)	895.9(4)	1126.7(2)
Z	4	4	2	2
ρ calcd (mg m^{-3})	1.325	1.618	1.590	1.780
Abs. coeff. (mm^{-1})	0.872	1.476	1.541	2.856
$F(000)$	2248	772	446	608
θ range (°)	2.7–28.0	2.7–34.5	2.7–26.5	3.2–29.0
Ref. collected/unique [$R(\text{int})$]	38 196, 6485 [0.120]	4364, 2843 [0.019]	5415, 1863 [0.091]	5154, 2966 [0.025]
Completeness (%)	99.6	98.8	99.9	99.2
Data/rest./param.	6485/0/323	2843/0/111	1863/0/119	2966/0/120
Gof on F^2	1.01	1.09	1.04	1.09
$R_1 [I > 2\sigma(I)]$	0.0601	0.0512	0.0585	0.0373
$wR_2 [I > 2\sigma(I)]$	0.1598	0.1314	0.1570	0.0928



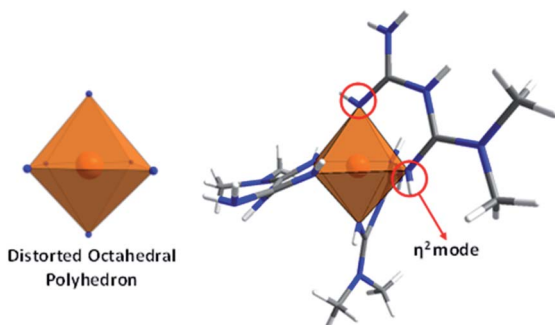


Fig. 2 Polyhedral representation and coordination mode of the ligand in the compound 1.

available to show the ionic behavior of the complexes. The crystallographic and refinement data are present in Table 1.

The $[\text{Co}(\text{C}_4\text{H}_{12}\text{N}_5)_3]\text{Cl}_2 \cdot \text{H}_2\text{O}$ compound (1) was obtained as cubic reddish crystals that crystallized in the $C2/c$ monoclinic space group with one molecule of the cationic complex, two chloride anions, and one molecule of water in the asymmetric unit (Fig. 1a). The cationic complex is present as a six-coordinated arrangement (CoN_6), generating a distorted octahedral polyhedron formed by three molecules of metformin in the chelate η^2 mode (Fig. 2).

The crystal packing of this compound is governed by electrostatic interactions between the ions and hydrogen interactions of the amine and methyl groups of the biguanidine ligand and water molecules with $\text{N2-H2A} \cdots \text{O1}$, $\text{O1-H1A} \cdots \text{Cl2}$, and $\text{N7-H7A} \cdots \text{Cl1}$ distances of 2.976(5), 3.127(4), and 3.185(5) Å, respectively (Fig. 3a). It is important to note that voids with a size of 667.6 \AA^3 able to accommodate up to 16 water molecules

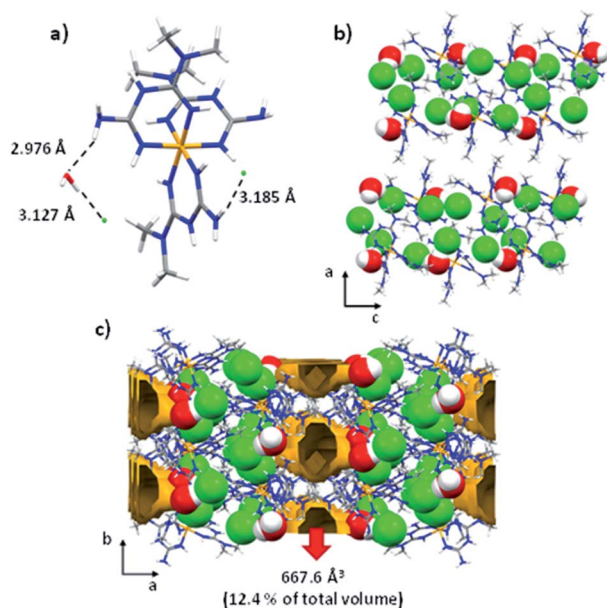


Fig. 3 (a) interactions of the secondary coordination sphere; (b) view in the ac plane of the chains, (c) crystal packing and voids along $[001]$ direction for the compound 1.

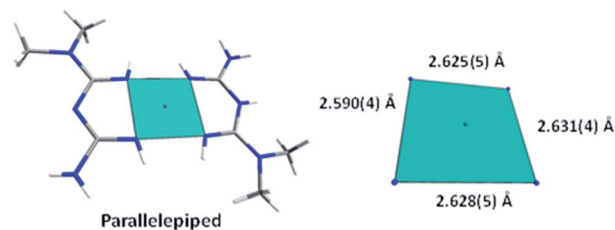


Fig. 4 Representation of the conformer A and the coordination polyhedron for the compound 2.

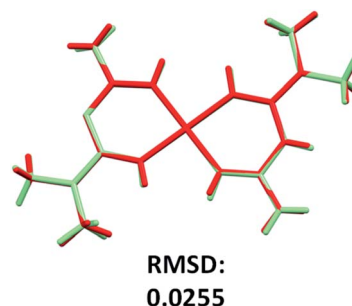


Fig. 5 Conformer representation and superposition of the conformer A (light green) and B (red), in the compound 2.

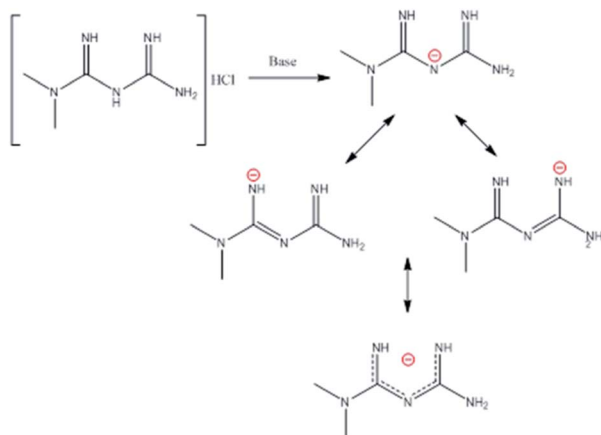
are present in the interlayer region (Fig. 3c). The disordered water molecules present in the voids join the layers giving rise to the formation of the 3D crystal packing of the complex.

The $[\text{Ni}(\text{C}_4\text{H}_{11}\text{N}_5)_2]\text{Cl} \cdot \text{H}_2\text{O}$ compound (2) was obtained as yellow crystals that crystallized in the $P2_1/c$ monoclinic space group. The compound contains two cationic complexes, two chloride anions, and two water molecules in the asymmetric unit (Fig. 1c). The complexes are formed by one metformin ligand and one deprotonated metformin coordinated to the Ni^{2+} center, forming a four-coordinated arrangement (NiN_4) with a distorted square planar polyhedron or parallelepiped (Fig. 4).

The two conformers observed in the asymmetric unit present slight differences in the size and torsion of the polyhedron edges. The torsion angle values were $0.862(13)^\circ$ and $-0.804(13)^\circ$ for conformer A and B, respectively. A root-mean-square deviation (RMSD) analysis of the atomic positions of the conformers was performed with a similarity value of 0.025 (Fig. 5).

In this compound, the deprotonation of metformin (metforminyde anion) in the secondary amine was observed. This deprotonation generates an increase in the imine $\text{C}=\text{N}$ bond length with values around 1.31 \AA in comparison with the neutral ligand (1.29 \AA). Furthermore, a decrease in the C1-N3 bond length of the secondary amine with values around 1.35 \AA was observed. Also, it was possible to compare the neutral metformin in the compound (2) and the compound $[\text{Ni}(\text{C}_4\text{H}_{11}\text{N}_5)_2](\text{-OH})\text{Cl}$ reported by Lemoine *et al.*,¹⁴ where the $\text{C}=\text{N}$ distances present values of $1.320(9)$ and $1.307(1) \text{ \AA}$, and values of C-N of $1.349(9)$ and $1.371(8) \text{ \AA}$. This behavior indicates a possibility of the formation of three resonant structures (Scheme 1) that stabilize the anion and enable the formation of the complex.





Scheme 1 Metformin reaction with and resonant structures of the anion metforminide.

The crystal packing of the Ni complex is formed by electrostatic interactions between the complex and the chloride anion. Along the [101] direction, the formation of chains by N8–H8...O2 and O2–H2D...N13 interactions with distances of 2.873(5) and 2.901(4) Å, respectively, was observed. The chains are joined by N–H...Cl interactions along [100] and [010] directions with distances around 3.34 Å (Fig. 6).

The $[\text{Cu}(\text{C}_4\text{H}_{12}\text{N}_5)_2]\text{Cl}_2 \cdot \text{H}_2\text{O}$ compound (3) was obtained as purple crystals, as previously reported by Lemoine *et al.*¹⁴ The asymmetric unit is formed by a half Cu^{2+} metallic cation located in a symmetry center, which is coordinated by one chelate metformin ligand, one chloride anion as a counter-ion, and one free water molecule. The complex is formed by the coordination of two chelate metformin ligands to generate a four-coordinated rectangular polyhedron (CuN_4). In this case, the sizes of the edges are 2.694(6) and 2.781(7) Å for the distances N1–N5 in the same ligand and N5–N1ⁱ between the ligands, respectively (Fig. 7).

Similar to the previous cases, the crystal packing is formed by electrostatic interactions between the cationic complex and

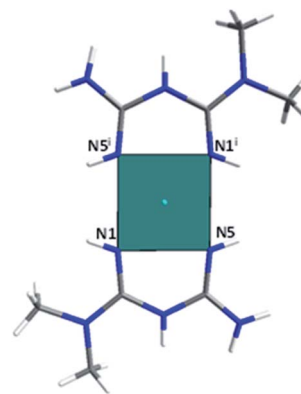


Fig. 7 Coordination polyhedron for the compound 3.

the chloride anions. In addition, we observed N1–H1...O1, O1–H1A...Cl1, N2–H2...Cl1, and N3–H3...Cl1 interactions with distances of 2.977(7), 3.098(5), 3.244(6), and 3.368(5) Å, respectively (Fig. 8a). These interactions allow the formation of layers in the plane (216) (Fig. 8b). The layers stack along the [101] direction by O1–H1B...Cl1 interactions with a distance of 3.172(5) Å giving rise to the crystal packing arrangement (Fig. 8c).

Finally, the compound $[\text{Zn}(\text{C}_4\text{H}_{11}\text{N}_5)\text{Cl}_3]$ (4) was obtained as colorless crystals, as previously reported by Zhu *et al.*¹⁶ with one Zn^{2+} metal coordinated by three chloride anions and one protonated metformin molecule in the asymmetric unit. The final complex presents a tetrahedral (ZnNCl_3) arrangement around the Zn center (Fig. 9).

Structurally, distortion in the protonated metformin ligand with a N4–C2–C1–N2 torsion angle of 93.13° is observed in comparison with values around 0° for the ligand in the previous complexes and 119.7° for the hydrochloride of metformin.²⁷ This behavior is due to a double bond loss of the imine and the formation of primary amines that induce a steric effect and distort the ligand (Fig. 9). In contrast to the structure reported by Zhu *et al.*,¹⁶ which proposed the formation of $\text{C}_4\text{H}_{12}\text{N}_5^+$ with the positive charge centered in the N coordinated to the zinc,

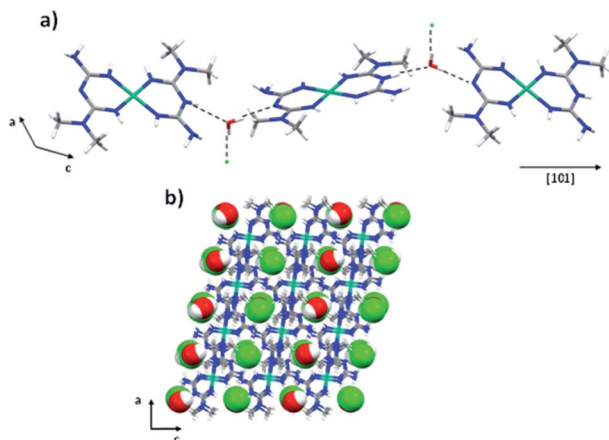


Fig. 6 (a) Chains formed along the [101] directions and (b) crystal packing of the $[\text{Ni}(\text{C}_4\text{H}_{11}\text{N}_5)_2]\text{Cl} \cdot \text{H}_2\text{O}$ compound.

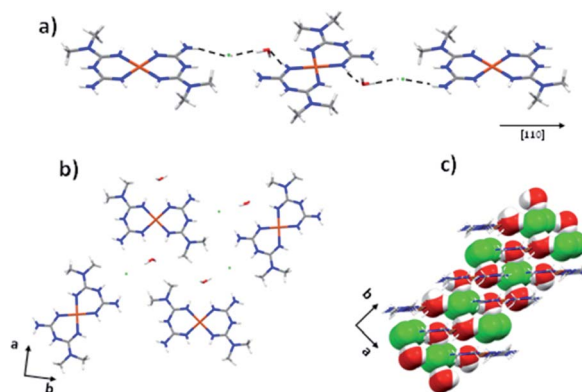


Fig. 8 (a) Interactions along [110] direction, (b) layers formed between the complex in the plane (216) and (c) crystal packing for the compound 3.



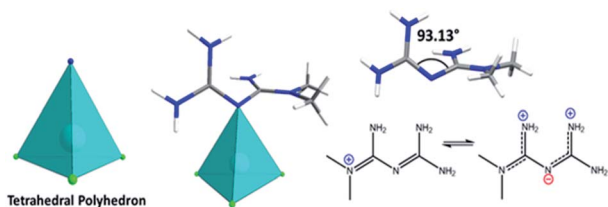


Fig. 9 Coordination polyhedron and distortion of the ligand in the compound 4.

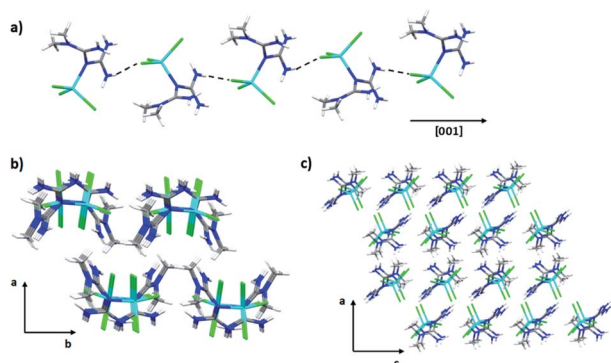


Fig. 10 (a) Cl \cdots H interactions along [001] direction, (b) interaction along [100] and [010] direction and (c) crystal packing for the compound 4.

indicating the formation of C=N⁺=C bond, we observed from the analysis of bond distances, asymmetric values in the C1–N3 and N3–C2 bonds with values of 1.343(3) and 1.378(4) Å, respectively. A N5–C2 bond distance decreasing, with a value of 1.300(3) Å, is associated with the formation of a double bond or resonance structure (Fig. 9).²⁸ Also, we observed distortion in the tetrahedral polyhedron due to differences in the Zn–Cl distances ranging between 2.242–2.259(9) Å, the distance Zn1–N3 with a value of 2.062(2) Å, and values of angles between 106.8–116.4°.

From the supramolecular point of view, the crystal packing is formed mainly by Cl \cdots H bonds. The formation of chains by halogen–hydrogen interactions along the [001] direction with N–H \cdots Cl distances of 3.368(3), 3.359(3), and 3.726(3) Å was observed (Fig. 10a). The formed chains are joined by N4–H4A \cdots Cl1 interactions with a distance of 3.359(3) Å. Finally, along the [010] direction, we also observed halogen interactions N1–H1B \cdots Cl3 with a distance of 3.372(2) Å (Fig. 10b) giving rise to the 3D crystal packing (Fig. 10c).

Supramolecular interactions analysis

To understand the supramolecular behavior of the obtained compounds, Hirshfeld surface (HS) and finger print plot analyses were performed. Hirshfeld surface analysis provides information about the regions in the molecule where interactions occur.²⁹ With this tool, it is possible to generate a surface d_{norm} map that shows (i) the interactions with distances less than the sum of the van der Waals radii as concave red regions

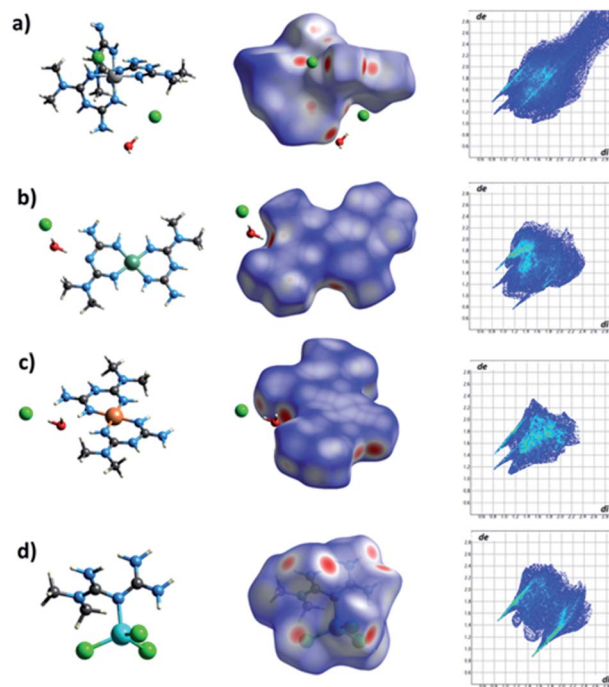


Fig. 11 Molecular representation, d_{norm} Hirshfeld surface and finger print plots for (a) [Co(C₄H₁₁N₅)₃]Cl₂·2H₂O, (b) [Ni(C₄H₁₁N₅)(C₄H₁₀N₅)]Cl·H₂O, (c) [Cu(C₄H₁₁N₅)₂]Cl₂·H₂O and (d) [Zn(C₄H₁₂N₅)Cl₃] compounds.

and (ii) the interactions equal to or greater than the sum of the van der Waals radii as white and blue regions, respectively.²⁹ In Fig. 11, it is possible to observe in the HS that the red regions are located on the donor–acceptor amine and imine groups. The finger print plots quantify the contribution of each interaction to the crystal packing (Fig. 11).³⁰

It is also possible to observe that in all the cases, the strongest and most important contributions to the crystal packing is given for N \cdots H, O \cdots H, and H \cdots Cl interactions, characterized by the presence of narrow peaks in the bottom of the finger print plots. In addition, we observed important interactions, including C \cdots H and H \cdots H, where the H \cdots H interactions are the more abundant interactions in the crystal packing (Fig. 12). Only in the Zn complex, we observed a high contribution of H \cdots

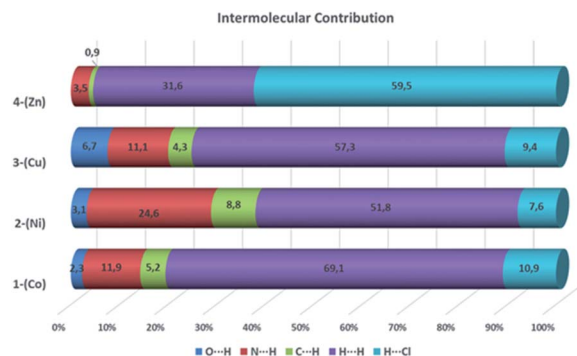


Fig. 12 Intermolecular contacts values for (1), (2), (3) and (4) compounds.



Cl interactions in the formation of the crystal packing. The different interaction values observed in all cases are characteristic of the nature of each complex and its crystal packing (Fig. 12).

Vibrational spectroscopy and thermal analysis

The interpretation of FTIR spectra was performed considering the most important internal vibrations of the functional groups in the complexes (ESI S1†). A N–H stretching vibration of the C=N–H group is observed in the region between 3100–3490 cm^{-1} for all compounds with high intensity.³¹ In $[\text{Co}(\text{C}_4\text{H}_{12}\text{N}_5)_3]\text{Cl}_2 \cdot \text{H}_2\text{O}$ (compound 1), the bands are overlapping by the O–H vibrations of the water molecules present in the structure.³² Two bands with medium-weak intensities in the region around 1470–1540 cm^{-1} are assigned to in-plane NH_2 deformation.³¹ In the region at 2800–3000 cm^{-1} , we observed symmetric and asymmetric stretching C–H vibrations of the methyl groups. The two peaks at 1570 and 1610 cm^{-1} are related to asymmetrical and symmetrical C=N vibrations. The peaks in the region around 1050–1250 cm^{-1} are assigned to C–N stretching of the aliphatic amine.³¹

The metal–metformin complexes show a similar thermal profile (ESI S2†) with an initial mass loss for free water of 6.87%, 5.8%, and 8.1% ($T_{\text{onset}} = 82, 67, 80^\circ\text{C}$) for compounds 1, 2, and 3, respectively. These mass losses are in agreement with the calculated values for two water molecules for 1 (6.72%) and 3 (8.3%) and one molecule for 2 (4.9%). The compounds 1, 2, 3, and 4 exhibit a decomposition temperature around 240 $^\circ\text{C}$, 312 $^\circ\text{C}$, 238 $^\circ\text{C}$, and 221 $^\circ\text{C}$ (T_{onset}), respectively.

Cytotoxicity test

C2C12 cell lines (mouse muscle) and HepG2 (human liver carcinoma) are widely used in the evaluation of the potential activity of new molecules with antidiabetic activity or different metabolic activity.³³ They are *in vitro* models that give preliminary information on the activity of specific molecules in reversing metabolic abnormalities in organs and or tissues involved in the establishment of diabetes.³⁴ Cell viability was evaluated using the MTT assay after the treatment of the three different compounds for 4 hours (C2C12) or 48 hours (HepG2) (Fig. 13). Compound 1 (Co) demonstrated a significant reduction (around 50%) in cell viability in both cell lines at concentrations of 500 and 1000 $\mu\text{g mL}^{-1}$. Compound 2 (Ni) reduced cell viability at concentrations $\geq 250 \mu\text{g mL}^{-1}$ in C2C12 cells and $\geq 62.5 \mu\text{g mL}^{-1}$ in HepG2 cells. Compound 3 (Cu) exhibited toxicity at concentrations $\geq 500 \mu\text{g mL}^{-1}$ in C2C12 cells and at 1000 $\mu\text{g mL}^{-1}$ in HepG2 cells (Fig. 13). Of note, it is impractical to develop therapeutic agents that must be administered at high concentrations. In addition, cell viability assays consider that a compound is safe, practicability values higher than 80%.³⁵ These results shows that compounds 1–3 exhibit low cytotoxicity at concentrations below 62.5 $\mu\text{g mL}^{-1}$ ($\sim 0.1 \text{ mM}$), and at a high concentration of 1000 $\mu\text{g mL}^{-1}$ ($\sim 1.8 \text{ mM}$), the cell viability is reduced in some cases around 50% in both cell lines. These results are consistent with different studies that evaluated the cell viability of metformin,^{36,37} indicating that the new compounds could potentially be used as safe drugs with minimal side effects. It is important to note that these tests are a preliminary evaluation of the viability of the compounds as safe drugs, and more studies must be conducted in order to know the effect of these molecules on healthy cells and the possible physiopathological mechanisms that intervene in the control of appetite, the increase in body weight and other associated metabolic factors.

Conclusions

In this work, we synthesized four compounds from the metformin ligand and divalent transition metals. The structural analysis reveals that all compounds crystallize in the monoclinic crystal system and centrosymmetric space groups, such as $C2/c$, $P2_1/c$, and $P2_1/n$. In addition, we observed different coordination modes and structural features of the metformin ligand, which depends on the protonation state of the ligand. For the first time, we reported an octahedral Co–metformin complex and a Ni–metformin–metforminyde planar square complex. The supramolecular analysis based on the Hirshfeld surface showed important differences between Co, Ni, and Cu compounds in comparison with the Zn compound. The three first complexes show a high contribution of $\text{H}\cdots\text{H}$ interactions compared with Zn, which shows a major contribution of $\text{H}\cdots\text{Cl}$ interactions to the crystal packing. In all structures, the $\text{N}\cdots\text{H}/\text{H}\cdots\text{N}$ play an important role in crystal packing in decreasing order of $\text{Ni} > \text{Co} > \text{Cu} > \text{Zn}$. C2C12 and HepG2 cells were treated with the Co, Ni, and Cu compounds, and cell viability was

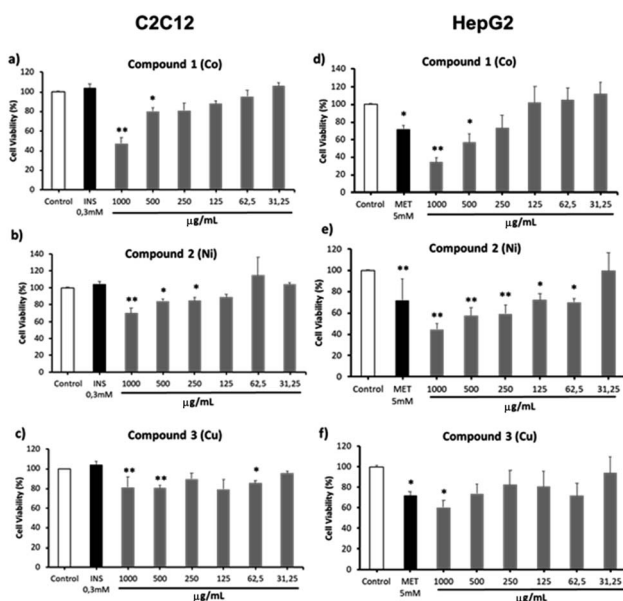


Fig. 13 Cytotoxicity of different molecules on cell lines C2C12 and HepG2. Cells seeded in 96-well plates were treated with the molecules for 4 h (C2C12) or 48 h (HepG2). The cytotoxicity was evaluated by MTT assay. Values are expressed as mean \pm SEM. ANOVA with *post hoc* Tukey for multiple comparisons was performed. ** $p < 0.01$; * $p < 0.05$. $n = 3$. Insulin 0.3 mM (INS) and metformin 5 mM (MET) are used as positive control.



evaluated using the MTT assay. The results demonstrate that the compounds exhibit low cytotoxicity at high concentrations.

Conflicts of interest

There are no conflicts to declare.

Acknowledgements

All authors acknowledge the Dirección General de Investigaciones from Universidad Santiago de Cali for the financial support (project no. 445-621118-146). S. V.-D. and J. E. are grateful to CAPES and CNPq (proc. #305190/2017-2), respectively, for the research fellowships.

Notes and references

- J. Dostou and J. Gerich, *Exp. Clin. Endocrinol. Diabetes*, 2001, **109**, S149–S156.
- W. Kerner and J. Brückel, *Exp. Clin. Endocrinol. Diabetes*, 2014, **122**, 384–386.
- G. Rena, D. G. Hardie and E. R. Pearson, *Diabetologia*, 2017, **60**, 1577–1585.
- S. R. Salpeter, E. Greyber, G. A. Pasternak and E. E. Salpeter, *Cochrane Database Syst. Rev.*, 2010, (4), CD002967.
- K. D. Mjos and C. Orvig, *Chem. Rev.*, 2014, **114**, 4540–4563.
- A. Sigel, H. Sigel, E. Freisinger and R. K. O. Sigel, *Metallo-Drugs: Development and Action of Anticancer Agents*, De Gruyter, Zürich, 2018.
- S. M. Abu-el-Wafa, M. A. El-Ries and F. H. Ahmed, *Inorg. Chim. Acta*, 1987, **136**, 127–131.
- S. S. Sharma, J. V. Ramani, D. P. Dalwadi, J. J. Bhalodia, N. K. Patel, D. D. Patel and R. K. Patel, *Eur. J. Chem.*, 2011, **8**, 723491.
- S. A. Fine and K. J. Kinsella, *US Pat.*, US20070196512A1, 1998.
- A. Levina and P. A. Lay, *Dalton Trans.*, 2011, **40**, 11675–11686.
- G. E. Gomez, R. F. D'Vries, D. F. Lionello, L. M. Aguirre-Diaz, M. Spinosa, C. S. Costa, M. C. Fuertes, R. A. Pizarro, A. M. Kaczmarek, J. Ellena, L. Rozes, M. Iglesias, R. Van Deun, C. Sanchez, M. A. Monge and G. J. A. A. Soler-Illia, *Dalton Trans.*, 2018, **47**, 1808–1818.
- G. L. Pardo Andreu, F. Z. D. Reis, M. González-Durruthy, R. D. Hernández, R. F. D'Vries, W. Vanden Berghe and L. C. Alberici, *Toxicol. in Vitro*, 2020, **63**, 104737.
- G. Montoya, G. Gutiérrez, R. D'Vries, J. Ellena and A. J. Panay, *J. Mol. Struct.*, 2018, **1173**, 937–941.
- P. Lemoine, M. Chiadmi, V. Bissery, A. Tomas and B. Viossat, *Acta Crystallogr., Sect. C: Cryst. Struct. Commun.*, 1996, **52**, 1430–1436.
- M. Zhu, L. Lu, P. Yang and X. Jin, *Acta Cryst. E*, 2002, **58**, m217–m219.
- M. Zhu, L. Lu, X. Jin and P. Yang, *Acta Crystallogr., Sect. C: Cryst. Struct. Commun.*, 2002, **58**, m158–m159.
- CrysAlisPro*, Oxford Diffraction/Agilent Technologies Ltd, Yarnton, Oxfordshire, England, 2014.
- G. Sheldrick, *Acta Crystallogr., Sect. A: Cryst. Phys., Diffraction, Theor. Gen. Crystallogr.*, 2015, **71**, 3–8.
- G. Sheldrick, *Acta Crystallogr., Sect. C: Struct. Chem.*, 2015, **71**, 3–8.
- O. V. Dolomanov, L. J. Bourhis, R. J. Gildea, J. A. K. Howard and H. Puschmann, *J. Appl. Crystallogr.*, 2009, **42**, 339–341.
- G. Sheldrick, *Acta Crystallogr., Sect. A: Cryst. Phys., Diffraction, Theor. Gen. Crystallogr.*, 2008, **64**, 112–122.
- A. Spek, *Acta Crystallogr., Sect. D: Biol. Crystallogr.*, 2009, **65**, 148–155.
- K. Brandenburg and H. Putz, *DIAMOND-Crystal and Molecular Structure Visualization, Crystal Impact*, Kreuzherrenstr, Bonn, Germany, 2006, vol. 102, p. 53227.
- C. F. Macrae, I. J. Bruno, J. A. Chisholm, P. R. Edgington, P. McCabe, E. Pidcock, L. Rodriguez-Monge, R. Taylor, J. Van De Streek and P. A. Wood, *J. Appl. Crystallogr.*, 2008, **41**, 466–470.
- C. Schmitz-Peiffer, D. L. Craig and T. J. Biden, *J. Biol. Chem.*, 1999, **274**, 24202–24210.
- M. B. Hansen, S. E. Nielsen and K. Berg, *J. Immunol. Methods*, 1989, **119**, 203–210.
- S. L. Childs, L. J. Chyall, J. T. Dunlap, D. A. Coates, B. C. Stahly and G. P. Stahly, *Cryst. Growth Des.*, 2004, **4**, 441–449.
- D. Kathuria, A. A. Bankar and P. V. Bharatam, *J. Mol. Struct.*, 2018, **1152**, 61–78.
- J. J. McKinnon, M. A. Spackman and A. S. Mitchell, *Acta Crystallogr., Sect. B: Struct. Sci., Cryst. Eng. Mater.*, 2004, **60**, 627–668.
- M. A. Spackman and J. J. McKinnon, *CrystEngComm*, 2002, **4**, 378–392.
- S. Gunasekaran, R. K. Natarajan, V. Renganayaki and S. Natarajan, *Indian J. Pure Appl. Phys.*, 2006, **44**, 495–500.
- Infrared and Raman Spectra of Inorganic and Coordination Compounds*, ed. K. Nakamoto, JOHN WILEY & SONS, INC., Hoboken, New Jersey, 2009.
- P. J. Mullen, B. Lüscher, H. Scharnagl, S. Krähenbühl and K. Brecht, *Biochem. Pharmacol.*, 2010, **79**, 1200–1209.
- A. Guillén, S. Granados, K. E. Rivas, O. Estrada, L. F. Echeverri and N. Balcázar, *Adv. Pharmacol. Sci.*, 2015, **2015**, 418673.
- I.O.S., Biological evaluation of medical devices – Part 5: tests for in vitro cytotoxicity. *International Organization for Standardization*: 2009; p. 34.
- O. N. Pyaskovskaya, D. L. Kolesnik, A. G. Fedorchuk, G. V. Gorbik and G. I. Solyanik, *Exp. Oncol.*, 2017, **39**, 264–268.
- Z. Gao, Z. Liu, M. Bi, J. Zhang, Z. Han, X. Han, H. Wang, G. Sun and H. Liu, *Exp. Ther. Med.*, 2016, **11**, 1700–1706.

